INTERSTITIAL POTENTIALS AND THEIR CHANGE WITH DEPTH INTO CARDIAC TISSUE

ROBERT PLONSEY AND ROGER C. BARR
Departments of Biomedical Engineering, Physiology, and Pediatrics, Duke University, Durham, North Carolina 27706

ABSTRACT The electrical source strength for an isolated, active, excitable fiber can be taken to be its transmembrane current as an excellent approximation. The transmembrane current can be determined from intracellular potentials only. But for multicellular preparations, particularly cardiac ventricular muscle, the electrical source strength may be changed significantly by the presence of the interstitial potential field. This report examines the size of the interstitial potential field as a function of depth into a semi-infinite tissue structure of cardiac muscle regarded as syncytial. A uniform propagating plane wave of excitation is assumed and the interstitial potential field is found based on consideration of the medium as a continuum (bidomain model). As a whole, the results are inconsistent with any of the limiting cases normally used to represent the volume conductor, and suggest that in only the thinnest of tissue (<200 μm) can the interstitial potentials be ignored.

INTRODUCTION

Electrocardiograms are, of course, measured with electrodes placed at the body surface. Surface electrograms are obtained from cardiac fibers lying in a tissue bath and are measured with electrodes placed in the bathing medium. Interstitial electrograms are obtained from within the ventricular walls, using electrodes that are mounted on a penetrating shaft. In all these cases, the measured potentials are regarded as samples of a potential field arising from cardiac electrical sources acting through an intervening volume conducting medium.

Because they are complicated, the effects of the intervening volume conducting medium have been evaluated by a simplification to one or another of two limiting extremes: One has been to treat each fiber as behaving like that of a single fiber in a uniform unbounded conducting medium, where currents spread as freely through radial as through longitudinal pathways. The other limiting case has been to envision a fiber deep within a multicellular structure, where currents could spread only along longitudinal pathways.

While each case could be a good approximation under limited circumstances, many in vivo or in vitro measurements arise under conditions that are not so clear cut. For example, how close to the endocardial surface must a ventricular fiber be before the electrophysiological sources are materially affected (if at all) by the highly conductive blood within the cavities? How many fibers must be present in a Purkinje strand before current flow loses the ability to easily flow radially into the surrounding volume?

Addressing such questions requires a quantitative evaluation of the changes in the effect of the volume conducting medium under circumstances that lie between the traditional limiting cases. The objective of this paper is to provide such an evaluation. The task is significantly simplified by using the properties of the bidomain model of cardiac tissue, since this permits the formulation of analytical expressions.

OVERALL STRATEGY

"Sources"

There are several ways of describing the distant electric field arising from active tissue. One can show that the solution is uniquely determined by the membrane currents through its relationship to the measured potentials by a set of transfer coefficients (Green's functions) based on calculations that include the interactions with the surrounding tissue and the enclosing medium (boundary conditions). Another way is to determine the electrical "sources" that, when immersed in a uniform conducting medium, will produce the observed effects. The advantage of the source formulation is that source-field relations are dual to electrostatic fields of charges and dipoles in free space. Consequently, they correspond to our usual way of thinking about and evaluating sources and their fields.

Geometry

The geometry used for the active tissue in this paper is that of a semi-infinite block. This is obviously different from that of any actual preparation, and as such does not directly provide the answers to any of the above questions. We use this geometry partly because it makes the analysis

of a complicated problem easier. However, it also has conceptual merit in its own right, since it is easy to identify the relative behavior of fields located deep within the sample, at the surface (and thereby in good contact with the surrounding isotropic conducting solution), and throughout a transition region.

Interstitial Potential Waveforms

Most of the analyses and results here are in terms of interstitial potential waveforms evaluated relative to a boundary between active tissue and an overlying isotropic conducting region. Although the essential elements of the results might also be expressed in terms of current flow pathways or volume conductor transfer coefficients, potential waveforms and their changes are used since they have an unambiguous meaning and are readily compared to experimental records. Furthermore, there is a more technical reason why examining the interstitial potential is advantageous. The limiting cases that now are used correspond to assuming the interstitial potential to be zero or have a simple relation to the intracellular potential, as reviewed briefly below. Examining the interstitial potential provides a means of determining the adequacy of such assumptions.

SINGLE FIBER IN AN UNBOUNDED MEDIUM

One of the limiting cases for which the effects of the intervening volume conductor is well established is that of a single fiber in a uniform unbounded conducting medium. For such a fiber, the flow of current across the fiber membrane into the surrounding medium constitutes a source for the extracellular field. If i_m is the current per unit length, then a current element $i_m dz$ behaves like a point source which (if we could forget the presence of the fiber itself) sets up an unbounded space field.

$$\Phi = \frac{1}{4\pi\sigma_e}\int_{-\infty}^{\infty}\frac{i_m dz}{r}, \tag{1}$$

where σ_e is the medium conductivity and r the distance from source element to the field point.

Eq. 1 can be obtained through a more rigorous development that requires the extracellular surface potentials be very small compared to intracellular, ($\Phi_e << \Phi_i$), a condition that appears to be ensured for isolated muscle and nerve fibers in unbounded media (2). In fact, this inequality is also the basis for setting the extracellular longitudinal resistance $r_e = 0$ in the linear core-conductor model resulting in (1)

$$i_m = \frac{1}{r_i}\frac{\partial^2\Phi_i}{\partial z^2} \approx \frac{1}{r_i}\frac{\partial^2 V_m}{\partial z^2}. \tag{2}$$

From Eqs. 1 and 2 the second derivative of the transmembrane potential can be interpreted as a line source density.

Despite the simplified conditions under which Eq. 1 is obtained, it has been applied to three-dimensional cardiac tissue (multicellular preparations) (3) element by element and it is of interest to examine the possible errors in doing so. A related study by Geselowitz et al. (4) considered the error in applying an unbounded free space lead field to a thin multicellular (anisotropic) cardiac tissue sample (and in this case discovered the anisotropy to have little effect).

MULTICELLULAR MODEL

The other limiting case where volume conductor effects have been evaluated in detail is when current flow is strictly longitudinal, as it is in some experimental preparations or under some circumstances in which the fiber is deep within a structure.

A multicellular preparation, viewed as consisting of many parallel fibers, is depicted in Fig. 1. Such a view would exactly characterize skeletal muscle tissue. Clerc (5) showed that such a structure also models cardiac muscle effectively. In fact, because of the syncytial nature of cardiac tissue, Fig. 1 can be used to represent propagation (or electrotonus) either along or even across the actual physical fiber direction (5).

If the fibers in Fig. 1 were bounded by a nonconductor (e.g., oil), then for identical axial propagation or electrotonus of all fibers the intracellular and interstitial currents would be essentially axial. Moreover, if the fibers and their distribution were uniform and if propagation were initiated synchronously at the same axial position, then every fiber would behave in exactly the same way.

Linear Core-Conductor Model

In particular, the electrical properties of the fibers of Fig. 1 can be described by the linear core-conductor model, as shown in Fig. 2. Among other important relations that arise from this model are those noted by Hodgkin and Rushton (6), namely, that

$$\Phi_i = \frac{r_i}{(r_i + r_e)}V_m \tag{3}$$

$$\Phi_e = -\frac{r_e}{(r_i + r_e)}V_m, \tag{4}$$

where r_e, r_i are the interstitial, intracellular resistance per unit length. The transmembrane current per unit length per fiber, i_m, then turns out to be (1)

$$i_m = \frac{1}{(r_i + r_e)}\frac{\partial^2 V_m}{\partial z^2}. \tag{5}$$

It is this expression, in fact, that is used by Geselowitz et al. (4) to evaluate the cardiac source in their tissue model. However, the conditions that lead to Eq. 5, namely intracellular and interstitial current that is both uniform and axial, cannot be true for fibers near the surface of a preparation in a tissue bath (or for fibers near a boundary

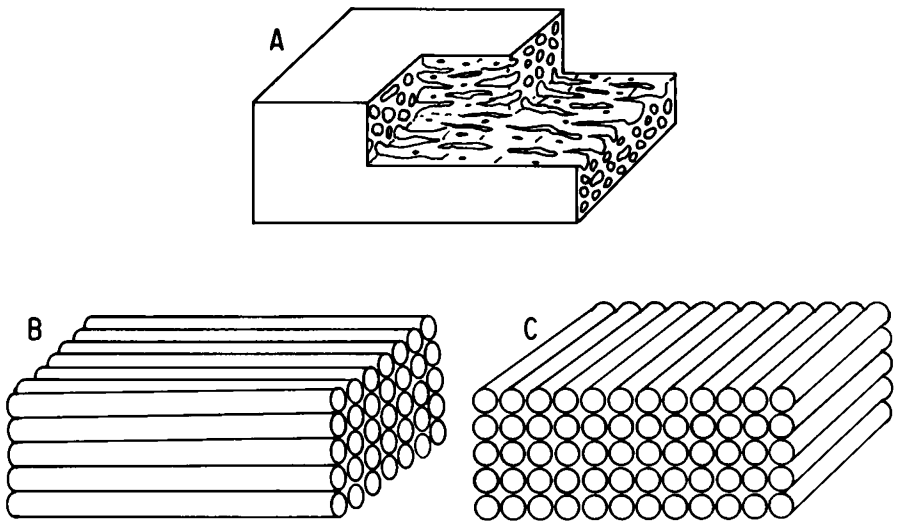

FIGURE 1 (*A*) Side view and cross-section of ventricular trabecular muscle showing the interconnection of cardiac cells facilitating uniform propagation (and action current flow) in any direction; (*B*) an equivalent linear model for longitudinal currents along fiber axis; and (*C*) across fiber axis. From Clerc (5).

of cardiac tissue in the whole heart), since interstitial current is actually not constrained to the axial direction.

SEMI-INFINITE TISSUE MODEL

This section contains a description of the geometric aspects of the model that will be used in this paper for investigating the transition between tissue deep within the structure and that in contact with a surrounding extracellular solution.

Model Description

Consider the semi-infinite model of cardiac tissue drawn in Fig. 3. We assume that the physical fibers lie in the z direction (in and out of the plane of the figure). Because actual propagation in the left ventricular free wall is mainly across fibers (7), we assume propagation is in the x direction. Following Clerc (5), we consider the tissue as if the fibers extended in the x direction (see Fig. 1).

We assume the applicability of the bidomain model (8), in which it is assumed that both intracellular and interstitial spaces are continuous (and uniform). Note that extracellular space within the tissue is referred to as interstitial to distinguish it from the extracellular medium that lies outside the tissue.

For a uniformly propagating plane wave in x, it is a good approximation that $V_m(t)$ is essentially the same everywhere (9). Consequently, the space-time field may be designated $V_m(t - x/\theta)$, where θ is the velocity. For a first order solution we have chosen θ to be a constant.

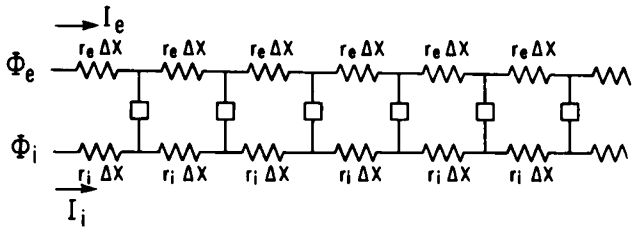

FIGURE 2 Linear core-conductor model of a fiber with intracellular resistance r_i per unit length and extracellular resistance r_e per unit length. The membrane is represented by an unspecified network that, under subthreshold conditions, can be modeled as a parallel $R_m/\Delta x$ and $C_m\Delta x$ element. Eqs. 3–5 depend on the assumption that intracellular and extracellular currents are axial (only).

Extension of Core-Conductor Model

The linear core-conductor model can be extended to a semi-infinite geometry. Doing so is worthwhile not only because the results are interesting in themselves, but also they can be compared with the more general results found below.

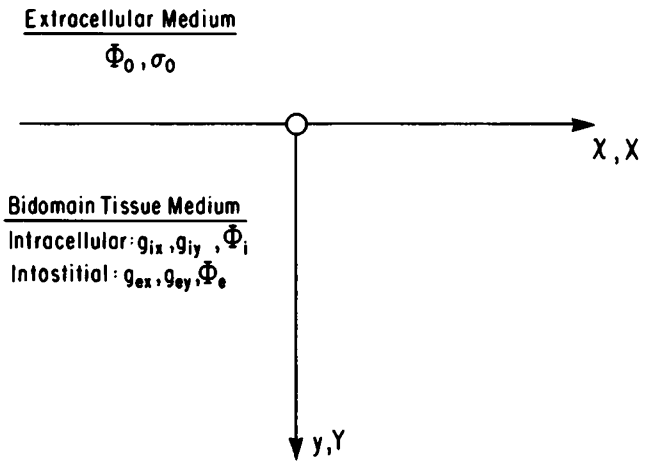

FIGURE 3 Semi-infinite uniform tissue extends from $0 < y < \infty$. Propagation in $+x$ direction with isochrones at x = constant. Because of assumed uniformity $\partial/\partial z = 0$.

We expect that for sufficiently large values of y (i.e., at a sufficient depth into the tissue) the presence of the extracellular space can be ignored in which case the intracellular and interstitial fields are governed by the linear core-conductor model; in particular Eqs. 3–5 apply. A consequence is that the exact (equivalent) axial dipole source expression for the field relative to the extracellular space (valid for single or multifibered preparations), namely, (2)

$$\Phi = \frac{1}{4\pi\sigma_e}\int \frac{\partial(\sigma_e\Phi_e - \sigma_i\Phi_i)}{\partial x}\nabla\left(\frac{1}{r}\right)\cdot\bar{a}_x\,dx\,dy\,dz, \qquad (6)$$

can be evaluated using Eqs. 3 and 4. One obtains

$$\Phi = \frac{\sigma_i A_i G}{4\pi}\int \frac{\partial V_m(x)}{\partial x}\nabla\left(\frac{1}{r}\right)\cdot\bar{a}_x\,dx\,dy\,dz, \qquad (7)$$

where

$$G = \frac{1}{\sigma_i A_i + \sigma_e A_e}, \qquad (8)$$

and A_i, A_e are the fractional intracellular, interstitial cross-sectional areas, while the integration is over the active tissue volume. In Eq. 8, G can be interpreted as the effective parallel conductance of the intracellular and interstitial paths (10). (In the above, reference is to the x component of cross-sectional area and conductivity.) The quantity $\partial V_m/\partial x$ in Eq. 7 is a line source density (which operates in a uniform medium of infinite extent).

A related question (which we will not consider here) is the local application of Eqs. 3 and 4 at isochrones that are not planar, since the alternative is to separately require Φ_i and Φ_e, a possibly difficult determination (11, 12).

ONE-DIMENSIONAL PROPAGATION IN SEMI-INFINITE CARDIAC TISSUE

Although the linear core-conductor model applies to the semi-infinite geometry at large depths into the tissue and leads to the useful result in Eq. 7, it is uncertain how large the depth, y, must be. If, say, y must exceed 1 cm, then since cardiac tissue itself is less in thickness, it is possible that Eqs. 3 and 4 do not apply to one-dimensional activation of real tissue.

Consequently, in this section we formulate a simple problem for which we can find an exact solution for $\Phi_e(x, y)$. The exact solution then can be compared to the result that is obtained by using the core-conductor model Eq. 4.

Longitudinal Currents

Referring to the geometry of Fig. 3, the bidomain longitudinal intracellular (subscript i) and interstitial (subscript e) currents are given by (8)

$$\bar{J}_i = -\left[g_{ix}\partial\Phi_i/\partial x\bar{a}_x + g_{iy}\partial\Phi_i/\partial y\bar{a}_y\right] \qquad (9)$$

$$\bar{J}_e = -\left[g_{ex}\partial\Phi_e/\partial x\bar{a}_x + g_{ey}\partial\Phi_e/\partial y\bar{a}_y\right]. \qquad (10)$$

The conductivity coefficients are defined on the total tissue space, as is characteristic of the bidomain model (8).

Function Ψ

Following Roth and Wikswo (13) we define a scalar function Ψ by

$$\Psi = \Phi_i + \frac{g_{ex}}{g_{ix}}\Phi_e = V_m + \frac{g_{ix} + g_{ex}}{g_{ix}}\Phi_e, \qquad (11)$$

where we have used $V_m = \Phi_i - \Phi_e$. We also impose a linear transformation to new coordinates X,Y where

$$X = x \qquad (12a)$$

$$Y = \sqrt{(g_{ix} + g_{ex})/(g_{iy} + g_{ey})}\,y. \qquad (12b)$$

Transmembrane Current

The transmembrane current can be found from the divergence of $\bar{J}_i$ or negative divergence of $\bar{J}_e$. Consequently,

$$\nabla\cdot(\bar{J}_i + \bar{J}_e) = 0. \qquad (13)$$

Substituting into Eq. 13 from Eqs. 9 and 10 results in

$$g_{ix}\frac{\partial^2\Phi_i}{\partial x^2} + g_{iy}\frac{\partial^2\Phi_i}{\partial y^2} + g_{ex}\frac{\partial^2\Phi_e}{\partial x^2} + g_{ey}\frac{\partial^2\Phi_e}{\partial y^2} = 0. \qquad (14)$$

Solution for $\nabla^2\Psi$

Using Eq. 11 allows conversion of Eq. 14 to

$$g_{ix}\frac{\partial^2\Psi}{\partial x^2} - g_{ex}\frac{\partial^2\Phi_e}{\partial x^2} + g_{iy}\frac{\partial^2\Psi}{\partial y^2} - \frac{g_{iy}g_{ex}}{g_{ix}}\frac{\partial^2\Phi_e}{\partial y^2} + g_{ex}\frac{\partial^2\Phi_e}{\partial x^2} + g_{ey}\frac{\partial^2\Phi_e}{\partial y^2} = 0. \qquad (15)$$

From Eq. 12 we now obtain

$$g_{ix}\frac{\partial^2\Psi}{\partial X^2} + g_{iy}\left(\frac{g_{ix} + g_{ex}}{g_{iy} + g_{ey}}\right)\frac{\partial^2\Psi}{\partial Y^2} + \left(g_{ey} - \frac{g_{iy}g_{ex}}{g_{ix}}\right)\frac{\partial^2\Phi_e}{\partial y^2} = 0. \qquad (16)$$

Substituting for Φ_e in Eq. 16 the value found in Eq. 11, and recalling that $\partial V_m/\partial y = 0$, gives finally

$$g_{ix}\frac{\partial^2\Psi}{\partial X^2} + g_{iy}\left(\frac{g_{ix} + g_{ex}}{g_{iy} + g_{ey}}\right)\frac{\partial^2\Psi}{\partial Y^2} + \left(\frac{g_{ix}g_{ey} - g_{iy}g_{ex}}{g_{ix}}\right)\left(\frac{g_{ix}}{g_{ix} + g_{ex}}\right)\left(\frac{g_{ix} + g_{ex}}{g_{iy} + g_{ey}}\right)\frac{\partial^2\Psi}{\partial Y^2} = 0 \qquad (17)$$

or

$$g_{ix}\frac{\partial^2\Psi}{\partial X^2} + \left(\frac{g_{ix} + g_{ex}}{g_{iy} + g_{ey}}\right)\left(g_{iy} + \frac{g_{ix}g_{ey} - g_{iy}g_{ex}}{g_{ix} + g_{ex}}\right)\frac{\partial^2\Psi}{\partial Y^2} = 0 \qquad (18)$$

or

$$\frac{\partial^2\Psi}{\partial X^2} + \frac{\partial^2\Psi}{\partial Y^2} = 0, \quad (Y > 0). \qquad (19)$$

From Eq. 11, and with $\nabla^2 \equiv \partial^2/\partial X^2 + \partial^2/\partial Y^2$, we have

$$\nabla^2\Psi = 0 = \nabla^2 V_m + \left(\frac{g_{ix} + g_{ex}}{g_{ix}}\right)\nabla^2\Phi_e. \tag{20}$$

Solution for Φ_e

Eq. 20 shows that Φ_e satisfies Poisson's equation in the transformed X,Y coordinate system. The classical solution to this equation in integral form (14) is

$$\Phi_e = -\left(\frac{g_{ix}}{g_{ix} + g_{ex}}\right)\frac{1}{2\pi}\int \nabla^2 V_m \ln(R)\mathrm{d}X'\,\mathrm{d}Y' \tag{21}$$

where

$$R = \sqrt{(X - X')^2 + (Y - Y')^2} \tag{22}$$

is the distance from a source point (X',Y') to a field point (X,Y).

Boundary between Tissue and Surrounding Medium

Eq. 21 gives the contribution to the interstitial potential field from the sources in the tissue (primary sources). However, the boundary condition at $y = 0$ must also be taken into account and this can be accomplished by the method of images (1). At $y = 0$, we have continuity of current requiring

$$g_{ey}\frac{\partial\Phi_e}{\partial y} = g_{ey}\sqrt{\frac{g_{ix} + g_{ex}}{g_{iy} + g_{ey}}}\frac{\partial\Phi_e}{\partial Y} = \sigma_0\frac{\partial\Phi_0}{\partial y} \tag{23}$$

where σ_0 is the conductivity of the isotropic extracellular conducting medium ($y < 0$). In addition, the continuity of potential at the boundary is required namely

$$\Phi_e(x, 0) = \Phi_0(x, 0). \tag{24}$$

Eqs. 23 and 24 will be satisfied if all sources are imaged at the mirror image point but with a relative amplitude, F, determined by the effective conductivity in $Y > 0$ (namely, from Eq. 23, $g_{ey}\sqrt{(g_{ix} + g_{ex})/(g_{iy} + g_{ey})}$) and the conductivity in $Y < 0$ (namely σ_0). The constant, F, is (1)

$$F = \frac{g_{ey}\sqrt{(g_{ix} + g_{ex})/(g_{iy} + g_{ey})} - \sigma_0}{g_{ey}\sqrt{(g_{ix} + g_{ex})/(g_{iy} + g_{ey})} + \sigma_0}. \tag{25}$$

Consequently, for field points in the tissue interstitial space of the region ($Y > 0$) we have

$$\Phi_e(X,Y) = -\frac{1}{2\pi}\left(\frac{g_{ix}}{g_{ix} + g_{ex}}\right)\left[\int_0^\infty\int_{X'}\frac{\partial^2 V_m}{\partial X'^2}\ln(R)\mathrm{d}X'\,\mathrm{d}Y' + F\int_{-\infty}^{0}\int_{X'}\frac{\partial^2 V_m}{\partial X'^2}\ln(R)\mathrm{d}X'\,\mathrm{d}Y'\right] \tag{26}$$

and R is from the integration (source) point to the fixed field point.

Elimination of Integration to Infinity

The evaluation of Eq. 26 requires one to use numerical procedures for approximating the double integrals. Because $\ln(R)$ increases without bound with increasing Y, it is not immediately obvious that the integral converges. The integral of $\partial^2 V_m/\partial X^2$ over X is zero since it equals $\partial V_m/\partial X$ evaluated at the plateau and resting regions, and, in each case, $\partial V_m/\partial X$ equals zero. Consequently, even though $\ln(R)$ increases without bound for $Y \to \infty$, the double-integral converges with integration over increasing values of Y, and a finite limit in the Y integration is satisfactory.

One can avoid this difficulty entirely by rearranging Eq. 26 in a way that eliminates the infinite integrals. For a field point with Y coordinate Y_1, Eq. 26 can be rewritten as

$$\begin{aligned}\Phi_e(X, Y_1) = -\frac{1}{2\pi}\left(\frac{g_{ix}}{g_{ix} + g_{ex}}\right)\Bigg[&\int_0^{Y_1}\int_{X'}\frac{\partial^2 V_m}{\partial X'^2}\ln(R)\mathrm{d}X'\,\mathrm{d}Y' \\ &+ \int_{Y_1}^{\infty}\int_{X'}\frac{\partial^2 V_m}{\partial X'^2}\ln(R)\mathrm{d}X'\,\mathrm{d}Y' \\ &+ F\int_{-\infty}^{Y_1}\int_{X'}\frac{\partial^2 V_m}{\partial X'^2}\ln(R)\mathrm{d}X'\,\mathrm{d}Y' \\ &- F\int_0^{Y_1}\int_{X'}\frac{\partial^2 V_m}{\partial X'^2}\ln(R)\mathrm{d}X'\,\mathrm{d}Y'\Bigg].\end{aligned} \tag{27}$$

In the second and third integrals the source constitutes exactly half of an infinite uniform double layer sheet; consequently, each contributes to the interstitial potential, a value given by the linear core-conductor equation divided by 2. Based on this, Eq. 27 becomes

$$\begin{aligned}\Phi_e(X, Y_1) = -\Bigg\{&\frac{1}{2}\left(\frac{g_{ix}}{g_{ix} + g_{ex}}\right)(1 + F)\,[V_m(X)] \\ &+ \frac{1 - F}{2\pi}\left(\frac{g_{ix}}{g_{ix} + g_{ex}}\right)\int_0^{Y_1}\int_{X'}\frac{\partial^2 V_m}{\partial X'^2}\ln(R)\mathrm{d}X'\,\mathrm{d}Y'\Bigg\},\end{aligned} \tag{28}$$

and $R = \sqrt{(X - X')^2 + (Y_1 - Y')}$. Eq. 28 not only avoids the infinite integrals of Eq. 26 but is generally easier to evaluate numerically. Furthermore, a physical interpretation of source-field relationships can be obtained, as will be discussed below.

Reduction to One Integral

A final approach to the evaluation of Eq. 26 is first to integrate by parts with respect to X'. The result is

$$\Phi_e(X,Y) = -\frac{1}{2}\left(\frac{g_{ix}}{g_{ix} + g_{ex}}\right)\left[\int_{-\infty}^{0}\int_{X'}\frac{\partial V_m}{\partial X'}\frac{(X - X')}{R^2}\mathrm{d}X'\,\mathrm{d}Y' + F\int_0^\infty\int_{X'}\frac{\partial V_m}{\partial X'}\frac{(X - X')}{R^2}\mathrm{d}X'\,\mathrm{d}Y'\right]. \tag{29}$$

In Eq. 29, but not Eq. 26, one can first integrate over Y' in the infinite interval. The result leaves a one-dimensional

integration, namely

$$\Phi_e(X,Y) = -\left\{\frac{1}{2}\left(\frac{g_{ix}}{g_{ix}+g_{ex}}\right)(1+F)\,[V_m(x)] - \left(\frac{1-F}{2\pi}\right)\left(\frac{g_{ix}}{g_{ix}+g_{ex}}\right)\int_{x'}\frac{\partial V_m}{\partial X'}\tan^{-1}\left(\frac{Y}{X-X'}\right)dX'\right\}. \quad (30)$$

From a computational standpoint Eq. 30 is superior to Eq. 26 or 28. Application of any of these Eqs. requires that the geometric coordinates be transformed correctly according to Eq. 12.

NUMERICAL METHODS

Inspection of the potentials can be accomplished by the numerical evaluation of Eqs. 26, 28, or 30, which permits an examination of $\Phi_e(X,Y)$ as a function of the parameter Y (distance from the surface). The results then can be compared with the limiting cases, e.g., compared with the potentials from Eq. 4 that are based on the core conductor model.

Accomplishing the numerical evaluation requires a numerical tabulation of an action potential, and of the conductivities. The following subsections show how we obtained each of these as idealizations of previous measurements in the literature.

Synthetic Action Potential

The shape and magnitude of the rising phase of a cardiac action potential is similar to the function

$$V_m(x) = 100e^{-8(x/\theta)^4} - 50, \quad x > 0$$
$$= 50, \quad x < 0, \quad (31)$$

where a uniform plateau is assumed for $x \le 0$, and where x is expressed in millimeters and θ in meters per second.[1] We also assume, in Eq. 31, that the temporal action potential is independent of velocity, in which case the spatial distribution depends on the velocity, θ, as shown. Consequently,

$$\frac{\partial^2 V_m}{\partial x^2} = 3{,}200\,(x^2/\theta^4)\,[32(x/\theta)^4 - 3]e^{-8(x/\theta)^4}, \quad x \ge 0. \quad (32)$$

A plot of V_m (Eq. 31), $\partial V_m/\partial x$, and $\partial^2 V_m/\partial x^2$ (Eq. 32) for θ = 0.2 m/s is shown in Fig. 4. Note that since the transformation of Eq. 12a is an identity; all expressions in terms of x and X are also identical.

[1] The resting potential of V_m is normally suppressed since its inclusion (or that of any constant term) contributes nothing to the evaluation of currents and potential fields (1). In Eq. 31 the introduction of −50mV also contributes nothing to subsequent calculations of Φ_e; its role is simply to reduce to zero, the total direct current (d.c.) component of $V_m(x)$. Its inclusion is simply a convenience since the derived expressions for $\Phi_e(x)$ will be seen to have zero d.c. component, and, consequently, its relationship to V_m through Eqs. 31 and 4 will require no subsequent adjustment for a possible d.c. component difference.

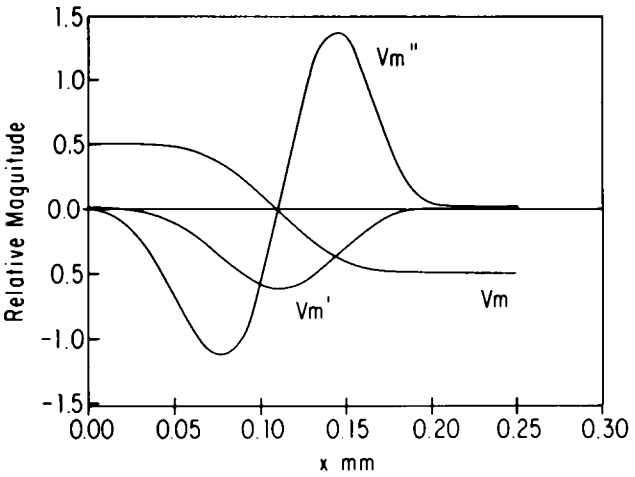

FIGURE 4 Behavior of $V_m(x)$, $\partial V_m/\partial x$, and $\partial^2 V_m/\partial x^2$ as functions of x for velocity of propagation, θ, of 0.2 m/s. Expressions are given in Eqs. 31 and 32.

Conductivities

For cross-fiber propagation we chose θ = 20 cm/s (3), and using the data derived from Clerc (5), but expressed in bidomain format (8), we have[2]

$$g_{ix} = 2.21 \times 10^{-5} S/mm \quad g_{iy} = 2.21 \times 10^{-5} S/mm \quad g_{iz} = 1.94 \times 10^{-4} S/mm \quad (33)$$

$$g_{ex} = 1.57 \times 10^{-4} S/mm \quad g_{ey} = 1.57 \times 10^{-4} S/mm \quad g_{ez} = 4.17 \times 10^{-4} S/mm. \quad (34)$$

Based on these values and on Eqs. 4 and 31 the core-conductor interstitial potential has a potential swing of $100 \times [0.221/(0.221+1.57)] = 12.3$ mV associated with the rising phase of V_m. The extracellular fluid was assumed to have a conductivity of 2×10^{-3} S/mm (resistivity of 50 ohmcm). These values lead to the parameter, F, defined in Eq. 25 having the value of −0.854. Note that because of the particular geometry of this example, and the equal transverse conductivities in x and y, Eq. 12b yields $Y = y$.

RESULTS

Using the parameters of Eqs. 33 and 34 in Eq. 26 permitted the potential fields at Y = 0, 0.05, 0.5, 5 mm to be evaluated. The same potential fields were confirmed using Eq. 30. The potentials are shown in Fig. 5. Also shown is the field that is predicted by the linear core-conductor model of Eq. 4.

In looking at the waveforms of the figure, one notes that each is drawn as a function of space (x). However, the assumption of constant propagation velocity implies that

[2] The values have been computed for an assumed 80% volume cell density rather than the 70% value assumed by Clerc.

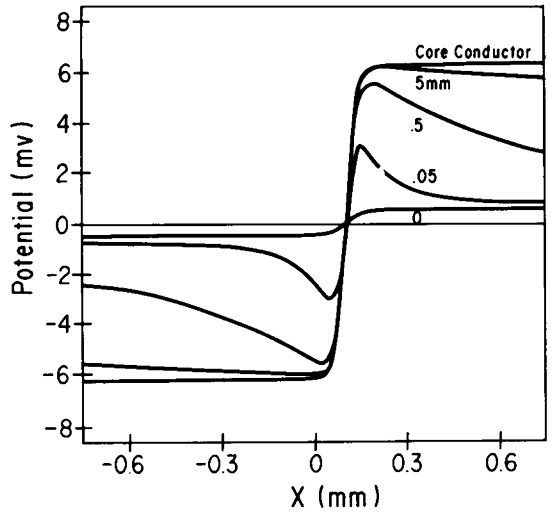

FIGURE 5 Plot of interstitial potential vs. axial distance, x, at different depths (as labeled) from interface of tissue with extracellular fluid.

the same waveforms would be computed as functions of time.

Limiting Potentials

Inspection of Fig. 5 shows that the potential waveform with the lowest amplitude corresponds to the field point at the surface, i.e., depth of zero into the tissue, as expected. Experimental waveforms made at the tissue surface always decline toward the baseline on their leading and trailing edges. The waveform shown does not do so as a result of the excitation wave extending infinitely deep.

At the other extreme, the largest waveform is that from the core-conductor model, as expected. This waveform is not expected to decline toward the baseline in its leading and trailing edges, since an infinitely long interval before and after the depolarization is assumed.

Changes with Depth

As depth increases (i.e., increasing Y), the interstitial potential departs from the shape of the surface waveform and approaches that predicted by Eq. 4 (i.e., the linear core conductor values). Note the sharp increase in the magnitude of the waveform for $Y = Y_1 = 0.05$ mm, whose peak is roughly six times the magnitude of the surface waveform. Moreover, the shape is markedly different. These effects are even more strongly present in the waveform at 0.5-mm depth. At a depth of 5 mm, however, the waveform is approaching its limiting magnitude, and the shape has returned to its original step appearance, though at a much larger magnitude.

Examination of Eq. 28 is helpful in indicating the cause of these changes with depth. At the surface ($Y_1 = 0$), the integral in Eq. 28 drops out and the potential distribution is seen to be proportional to $V_m(x)$. Therefore, at the surface the potential has a peak magnitude of $0.5 \times 6.2 \times 0.146 = 0.45$ mV, as seen in the plot in Fig. 5.

At increasing values of Y the contribution from the first term in Eq. 28 remains the same. Modifications are introduced by the additional (integral) expression in Eq. 28.

The integral can be viewed as generating an interstitial field due to a dipole source density that lies in the confined region $0 < Y < Y_1$, and in the range of X over which $\partial V_m/\partial X \neq 0$. For small Y_1 the source extent is small and this field is consequently small and falls off rapidly with increasing X-distance from the sources. For large Y_1 the integral contributes substantially to the total amplitude, while its influence extends to large values of X (to a distance comparable to the Y_1).

At a large depth into the tissue, which from Fig. 5 appears to be a depth of $Y = 0.5$ mm or more, the interstitial field is essentially the same as that given by the linear core-conductor model, at least out to the $X = \pm 1.0$ mm that is plotted. According to Eqs. 4, 33, and 34 the core-conductor magnitude should be equal to $12.3/2 = 6.15$ mV, as calculated earlier, a value that is correctly reflected in Fig. 5.

DISCUSSION

Relation to Experimental Findings

While some aspects of this paper deal with conceptual and mathematical points that are interesting in their own right, all the particular aspects of the model and the analysis are closely tied to well established experimental results, expressed in mathematical form, as cited specifically in each section. As such it is to be expected that the numerical results should correspond to actual measurements except for discrepancies caused by the assumption here of an infinitely deep excitation wave. There are, of course, a large number of reported experimental recordings of electrograms measured at varying depths in many different tissue preparations. However, recordings that might be compared with the results presented here in a detailed way do not yet exist, other than for the limiting cases.

As for the latter, Spach and Dolber (15) (see their Fig. 4) show around 1.5-mV peak-to-peak surface potential for transverse propagation (compare with 0.9 mV in this simulation) and 6.5-mV surface potential for longitudinal propagation. For longitudinal propagation, if Eqs. 33, 34, and 28 are used, one obtains 4.0-mV peak-to-peak surface potential. Since the measurements are taken on their tissue, they can only be compared in an approximate sense, of course.

For potentials at a "large" depth the simulated values are 12.3 mV, peak-to-peak, for transverse propagation, as discussed earlier, while using Eqs. 33, 34, and 4 one evaluates 31.7 mV for longitudinal propagation. Measured

values in the literature normally do not assess the nature of anisotropic propagation at deep measurement sites; however, typical amplitude values of 27 mV, peak-to-peak, are obtained (16).

Source-field Equations

Discussion of the results is aided by using the rigorous source-field Eq. 6 given earlier. This equation can be reformulated as (2)

$$\Phi = \frac{1}{4\pi\sigma_e}\int dS \int \left[\sigma_e \frac{\partial \Phi_e}{\partial x} - \sigma_i \frac{\partial \Phi_i}{\partial x}\right] \bar{a}_x \cdot \nabla\left(\frac{1}{r}\right) dx, \quad (35)$$

and the term in brackets can be interpreted as an axial dipole source density. The total dipole source, D, from a region of extent $x_1 < x < x_2$ is then simply,

$$D = \sigma_e[\Phi_e(x_2) - \Phi_e(x_1)] - \sigma_i[\Phi_i(x_2) - \Phi_i(x_1)]. \quad (36)$$

Limiting Cases

It is interesting to examine quantitatively the regions over which the traditional limiting cases provide an accurate approximation to these results.

Close Contact with an Unbounded Medium. This limiting case is clearly a good approximation when the extracellular potential is near zero. It is clear from Fig. 5 that the assumption of $\Phi_e = 0$ is not well justified even for fairly superficial sites. In fact, it is remarkable how rapidly Φ_e grows with depth, even at depths of only 200 μm.

What about formulations that ignore the interstitial space altogether? Such formulations amount to dropping the first term in Eq. 35 and replacing Φ_i by V_m. What is ignored are the sources associated with the changes in Φ_e, as described in Fig. 5. For the numerical values chosen, which represent typical normal physiology, the error amounts to neglecting changes in Φ_e that are 20% of the changes in V_m (or 25% the change in Φ_i). Since $\sigma_e/\sigma_i \approx 8$ (5), this percentage is augmented and represents a very substantial error in the application of Eq. 35. Consequently, only tissue that is very thin (possibly < 200 μm) can be considered essentially free of this error.

Core Conductor Assumptions. On the other hand, the peak values of Φ_e rapidly approach those required by the core-conductor model at small depths. Thereby the core-conductor model rapidly becomes a good approximation at only very small depths. However, the potential increasingly differs from core-conductor predictions for increasing distance ahead and behind the excitation wavefront (increasing x). One can interpret changes in Φ_e as a direct measure of the net source (dipole). On this basis it seems reasonable to use the core-conductor model to analyze sources in the neighborhood of the rising phase of V_m using the core-conductor assumptions. Away from this region a correction appears necessary.

More specifically, the field from sources arising from the phase zero region is described by Eqs. 7 and 8, but diffused additional sources must be assigned in the lateral space. The importance of the latter depends to some extent on source-field distance; it will be negligible if the source-field distance is small compared with the extent of the lateral source region. And the extent of the lateral source increases with increasing tissue thickness as is evident from Fig. 5.

Tissue of Finite Thickness

One could use the results of Fig. 5 to guess at the treatment of tissue of finite thickness. For example, in a tissue sample 1-mm thick, the behavior of Φ_i,Φ_e, and V_m could be expected to be governed by the core-conductor relations, Eqs. 3 and 4, in the region of the rising phase but deviate somewhat from this in the regions on either side. The interstitial field in the latter regions should approach that at the surface rather than hold at the core-conductor value.

This work was supported by grant HL-11307 from the National Institutes of Health and ECE-8514278 from the National Science Foundation.

Received for publication 21 April 1986 and in revised form 2 September 1986.

REFERENCES

1. Plonsey, R. 1969. Bioelectric Phenomena. McGraw-Hill Book Co., New York.
2. Plonsey, R. 1974. The active fiber in a volume conductor. *IEEE (Inst. Electr. Electron. Eng.) Trans. Biomed. Engr.* BME-21:371–381.
3. Spach, M. S., W. T. Miller III, E. Miller-Jones, R. B. Warren, and R. C. Barr. 1979. Extracellular potentials related to intracellular action potentials during impulse conduction in anisotropic canine cardiac muscle. *Circ. Res.* 45:188–204.
4. Geselowitz, D. B., R. C. Barr, M. S. Spach, and W. T. Miller III. 1982. The impact of adjacent isotropic fluids on electrocardiograms from anisotropic cardiac muscle. *Circ. Res.* 51:602–613.
5. Clerc, L. 1976. Directional differences of impulse spread in trabecular muscle from mammalian heart. *J. Physiol. (Lond.).* 255:335–346.
6. Hodgkin, A. L., and W. A. H. Rushton. 1946. The electrical constants of crustacean nerve fiber. *Proc. R. Soc. Lond. Biol. Sci.* 133:444–479.
7. Durrer, D. 1970. Total excitation of the isolated human heart. *Circulation.* 41:399–912.
8. Plonsey, R., and R. C. Barr. 1984. Current flow patterns in two-dimensional anisotropic bisyncytia with normal and extreme conductivities. *Biophys. J.* 45:557–571.
9. Plonsey, R. 1974. An evaluation of several cardiac activation models. *J. Electrocardiol. (San Diego).* 7:237–244.
10. Pilkington, T. C., and R. Plonsey. 1982. Engineering Contributions to Biophysical Electrocardiography. IEEE Press, John Wiley & Sons, Inc., New York. 35–37.
11. Barr, R. C., and R. Plonsey. 1984. Propagation of excitation in idealized anisotropic two-dimensional tissue. *Biophys. J.* 45:1191–1202.
12. Muller, A. M., and V. S. Markin. 1978. Electrical Properties of

nerve-muscle syncytia-III. Steady form of the excitation front. *Biophysics*. 22:699–704.

13. Roth, B. J., and J. P. Wikswo, Jr. 1985. A bidomain model for the extracellular potential and magnetic field of cardiac tissue. *IEEE (Inst. Electr. Electron. Eng.) Trans. Biomed. Eng.* BME-33:467–469.
14. Morse, P. M., and H. Feshbach. 1953. Methods of Theoretical Physics. McGraw-Hill Book Co., New York.
15. Spach, M. S., and P. C. Dolber. 1986. Relating extracellular potentials and their derivatives to anisotropic propagation of a microscopic level in human cardiac muscle. *Circ. Res.* 58:356–271.
16. Spach, M. S., and R. C. Barr. 1975. Ventricular intramural and epicardial potential distributions during ventricular activation and repolarization in the intact dog. *Circ. Res.* 37:243–257.